Sunlight-assisted hydrogenation of CO_2 into ethanol and C2+ hydrocarbons by sodium-promoted Co@C nanocomposites

Lichen Liu[a], Alberto V. Puga[a], Jorge Cored[a], Patricia Concepción[a], Virginia Pérez-Dieste[b], Hermenegildo García[a,*], Avelino Corma[a,*]

[a] Instituto de Tecnología Química, Universitat Politècnica de València-Consejo Superior de Investigaciones Científicas (UPV-CSIC), Avenida de los Naranjos s/n, 46022, Valencia, Spain
[b] ALBA synchrotron light source, 08290, Cerdanyola del Vallès, Barcelona, Spain

ABSTRACT

The hydrogenation of CO_2 into hydrocarbons promoted by the action of sunlight has been studied on Co nanoparticles covered by thin carbon layers. In particular, nearly 100% selectivity to hydrocarbons is obtained with increased selectivities towards C2+ hydrocarbons and alcohols (mainly ethanol) when using nanostructured materials comprising metallic cobalt nanoparticles, carbon layers, and sodium as promoter (Na-Co@C). In the contrary, larger amount of CH_4 and lower selectivity to C2+ hydrocarbons and alcohols were obtained in the conventional thermal catalytic process. When using Co@C nanoparticles in the absence of Na or bare Co_3O_4 as catalyst, methane is essentially the main product (selectivity > 96%). Control experiments in the presence of methanol as a hole scavenger suggest the role of light in generating charges by photon absorption as promoting factor. The reaction mechanism for photoassisted CO_2 hydrogenation on the Co-based catalysts was investigated by near ambient-pressure X-ray photoelectron (AP-XPS) and in situ Raman spectroscopies, which provided information on the role of light and Na promoter in the modulation of product distribution for CO_2 hydrogenation. Spectroscopic studies suggested that surface CO_2 dissociation to CO, the stabilization of CO adsorbed on the surface of Na-Co@C catalyst and the easy desorption of reaction products is a key step for photothermal CO_2 hydrogenation to ethanol and C2+ hydrocarbons.

1. Introduction

Photocatalytic CO_2 reduction is one of the most challenging issues in chemical research [1]. In numerous investigations in this area, CO_2 reduction is coupled with the splitting of H_2O for the production of solar fuels, a process which is commonly referred to as artificial photosynthesis [2,3]. However, with heterogeneous photocatalysts, reaction rates for the transformation of CO_2/H_2O mixtures are usually in the order of micromoles per hour, which is too far from any practical application [4–7]. Moreover, the major products in most of the reports dealing with artificial photosynthesis are frequently CH_4 or CO. It appears that with the heterogeneous catalytic systems reported so far, it is very difficult to achieve carbon chain growth to go beyond CH_4 and to produce significant amounts of more valuable C2+ hydrocarbons during the photocatalytic reduction of CO_2.

As an alternative to the reduction of CO_2 by H_2O, in the past few years, our research group has reported the photoassisted hydrogenation of CO_2 to CH_4 on Ni (or NiO) nanoparticles under solar light irradiation

[8,9]. The formation rate of CH_4 was as high as mmol/h, which is about three orders of magnitude higher than for typical $CO_2 + H_2O$ reactions. However, only CH_4 was selectively produced using Ni, NiO or other supported Group VIII catalysts [10]. In a recent work, Ozin and his coworkers reported that hydride-terminated Si nanoparticles can catalyze the reverse water-gas shift (RWGS) reaction leading to the formation of CO under photo-thermal conditions [11]. Iron nanoparticles encapsulated in carbon can also be efficient catalyst for the photoassisted RWGS reaction, as reported by Ye and co-workers [12]. However, in most of previous works, the selectivities to C2+ products are usually quite low. In a recent work, Zhang et al. have reported the application of CoFe@C bimetallic nanoparticles for CO_2 hydrogenation to hydrocarbons by a photothermal process [13]. It has been claimed that solar light irradiation can increase the temperature of the catalyst surface, which further enhances the activity. However, the influence of solar light irradiation on the reaction mechanism for CO_2 hydrogenation is not clear [14,15].

The lack of photoassisted processes generating C2+ hydrocarbons

contrasts with conventional heterogeneous catalysis, whereby mixtures of CO_2 and H_2 can be transformed into CO or CH_4, but interestingly, also into other C2+ hydrocarbons, depending on the catalyst [16–20]. For instance, metal nanoparticles (including Ni, Co and Ru materials) are active catalysts for CO_2 methanation, converting CO_2 to CH_4 [21–23]. This reaction requires temperatures above 250 °C, giving rise to a large amount of CO (in some cases, selectivity to CO can be as high as 80%) as by-product. Moreover, metal nanoparticles (including Fe, Co and Ru materials) can also serve as active catalysts for Fischer-Tropsch synthesis (FTS), transforming CO/CO_2 and H_2 into hydrocarbons and oxygenates, though FTS is usually performed at high pressure [24]. Recently, it has also been reported that Ni-NiO$_x$ nanocomposites can catalyze the CO hydrogenation into hydrocarbons by a photoassisted process [25].

In this work, we report the photothermal hydrogenation of CO_2 into hydrocarbons (CH_4 together with a high proportion of C2+ hydrocarbons and ethanol) using Na-promoted Co@C nanocomposites as catalysts under solar light and near-atmospheric pressure. The reaction rate of this process is in the order of mmol $g_{cat}^{-1}h^{-1}$ and the selectivity to ethanol is 6.5% at 37% CO_2 conversion and > 30% selectivity to C2+ hydrocarbons at nearly 100% CO_2 conversion. It will also be shown that the analogous thermal reaction with the same catalyst behaves differently and produces larger amounts of CH_4 and much less alcohols. The effect of light irradiation on the reaction mechanism has been studied by ambient-pressure X-ray photoelectron spectroscopy (AP-XPS) and in situ Raman spectroscopy. The results indicate that light has a clear effect on the formation and stabilization of intermediates for the production of ethanol and the C-C chain growth process for the production of C2+ hydrocarbons.

2. Experiments

2.1. Catalyst preparation

2.1.1. Preparation of Na-Co@C

The sodium-promoted Co@C nanocomposites were prepared through the reduction of cobalt-sodium-ethylenediaminetetraacetate (Co-Na-EDTA) complexes by H_2. The Co-EDTA complex was prepared through a hydrothermal process. Firstly, Na_2EDTA (4.47 g) and NaOH (0.96 g) were dissolved in H_2O (20 mL) at room temperature. $Co(NO_3)_2$ (6.98 g) was added to the above solution under strong stirring, resulting in formation of homogeneous solution. Then, methanol (10 mL) was added to the aqueous solution. A portion of the resulting purple homogeneous solution (*ca.* 23 mL) was transferred into a 35 mL stainless steel autoclave and kept in an oven at 200 °C for 24 h. After cooling to room temperature, the solid precipitates were collected by filtration and washed with deionized water and acetone, followed by drying at 60 °C to yield the Co-EDTA complex. Then, the sodium-promoted Co@C nanocomposite (Na-Co@C) was obtained by reduction of Co-EDTA complex with H_2 at 450 °C for 2 h with a ramp rate of 10 °C/min from room temperature to 450 °C.

2.1.2. Preparation of Co@C

In the first step, 0.5 g of Co_3O_4 nanoparticles were prepared as precursor for Co@C. $Co(OAc)_2$ (4.94 g) was dissolved in ethylene glycol (100 mL) under stirring at 160 °C. When $Co(OAc)_2$ was totally dissolved in ethylene glycol, an aqueous Na_2CO_3 solution (mixture of 4.24 g of Na_2CO_3 and 160 mL distilled water) was added drop by drop. It took 1.5~2 h to finish the process, and then, the suspension was aged for another 1 h at 160 °C before cooling down to room temperature. A purple solid product was obtained after the filtration of the suspension and washing with water and acetone. After drying in an oven at 60 °C for 16 h, the solid product was submitted to calcination in static air at 450 °C for 3 h with a ramp rate of 1 °C/min from room temperature to 450 °C, resulting in formation of Co_3O_4 nanoparticles. In the second step, Co@C sample was prepared through a carbon coating process

using the Co_3O_4 nanoparticles as precursor. Glucose (360 mg) was dissolved in distilled water (20 mL). Then Co_3O_4 (0.5 g) was dispersed in the glucose aqueous under ultra-sonication. The black suspension was transferred into autoclave and kept at 175 °C for 18 h. After cooling down to room temperature, the solid product was washed with water and acetone and dried in oven at 60 °C, resulting in the formation of Co$(OH)_2$/C composites. The Co@C nanoparticles were obtained by annealing the Co$(OH)_2$/C composites in N_2 at 600 °C for 2 h at a ramp rate of 10 °C/min from room temperature to 600 °C. After being kept at 600 °C for 2 h, the sample was cooled down in N_2 flow to room temperature and stored in glass vial in the ambient environment.

2.2. Structural characterization techniques

Samples for electron microscopy studies were prepared by dropping the suspension of the powder sample using CH_2Cl_2 as the solvent directly onto holey-carbon coated nickel or copper grids. All the measurements were performed in a JEOL 2100 F microscope operating at 200 kV both in transmission (TEM) and scanning-transmission modes (STEM). STEM images were obtained using a High Angle Annular Dark Field detector (HAADF), which allows Z-contrast imaging. Powder X-ray diffraction (XRD) was performed using a HTPhilips X'Pert MPD diffractometer equipped with a PW3050 goniometer using Cu Kα radiation and a multisampling handler.

2.3. Ambient-pressure X-ray photoelectron spectra (XPS)

The AP-XPS experiments were performed at the CIRCE beamline of the ALBA synchrotron. CIRCE is an undulator beamline with a photon energy range 100–2000 eV. The beam spot size at the sample is $100 \times 30 \, \mu m^2$. The AP-XPS endstation, equipped with a PHOIBOS 150 analyzer from SPECS, is described elsewhere. [26] The data were acquired with an instrumental energy resolution better than 0.3 eV, PE 20 eV and exit slit 20 μm. The sample (10 mg) was pelletized and mounted onto the sample holder using a resistive bottom heater for sample heating. The temperature was monitored during all experiments with a K-type thermocouple in direct contact with the sample. For the photothermal studies a solar simulator (Newport®, Oriel Instruments, model 69,921, same as for the catalytic studies) was placed outside on top of a viewport front to the sample. CO_2 and H_2 were fed into the analysis chamber using two leak valves maintaining a constant pressure of 0.1 mbar CO_2 and 0.5 mbar H_2 inside the chamber. The AP-XP spectra were acquired using two different photon energies, 510 and 1000 eV. XPS data were analyzed using the CASA software. The atomic fraction of each element was obtained from the peak areas, calibrated for the incident photon flux and the corresponding cross sections.

2.4. Operando Raman studies

Raman spectra were recorded at ambient temperature with a 785 nm HPNIR excitation laser on a Renishaw Raman Spectrometer ("Reflex") equipped with an Olympus microscope and a CCD detector. The laser power on the sample was 15 mW and a total of 20 acquisitions were taken for each spectrum. For the *operando* Raman experiments 20 mg of sample was loaded into a quartz cell adequate for "in situ" Raman studies. After evacuating the cell (P < 10 mbar), CO_2, N_2 and H_2 in a 1:1:5 M ratios were introduced up to a total pressure of ~1 bar. In the photothermal studies, the catalytic cell was irradiated using a solar simulator (Newport®, Oriel Instruments, model 69,921). Light irradiation was stopped at specific times where Raman spectra were acquired. For the thermal studies the catalytic cell was introduced in a heating plate at 235 °C. Raman spectra were acquired under reaction conditions at specific times.

2.5. CO₂ hydrogenation tests

Photothermal CO_2 hydrogenation under simulated sunlight irradiation in the presence of the catalyst solid powders (75 mg) were carried out in a purpose-designed quartz cell (V = 50 cm³). After evacuating the cell (P < 10 mbar), appropriate amounts of CO_2, N_2 and H_2 (typically, 20, 20 and 100 cm³ as standard conditions) were introduced with a final pressure of ~2.8 bar. Simulated sunlight irradiations of the solids were carried out using a solar simulator (Newport®, Oriel Instruments, model 69,921) equipped with a Xe lamp (1000 W) coupled with an AM1.5 filter that provides simulated concentrated sunlight. Unless otherwise noted, the irradiance at the surface of the solids was *ca.* 24 kW m⁻².

The initial reaction rates of Na-Co@C sample under thermal or photothermal conditions were measured in a photoreactor composed of a quartz tube (V = 300 cm³) and a built-in heating plate, using the same gaseous mixture as described above, at a total pressure of *ca.* 100 kPa. The reactor body is made of aluminium to favor heat transfer to the environment and no special cooling system was used. The temperature and pressure inside the photoreactor were measured by an internal thermocouple and a manometer, respectively.

The time-profile conversion of the reactions was followed by analyzing samples (*ca.* 2.5 cm³) taken from the gas phase periodically on a two-channel chromatograph (Agilent 490 Micro GC, carrier gas: Ar) equipped with thermal conductivity detectors (TCD), and a MS 5 Å column (first channel) for the quantification of H_2, N_2 and CO, and a PoraPLOT Q column (second channel) for the quantification of CO_2 and hydrocarbons. The analysis of C2+ hydrocarbons and oxygenates was performed with a SCION-456 GC with FID detector. The selectivity to different products is calculated based on the carbon.

3. Results and discussion

3.1. Synthesis and structural characterization of Na-promoted Co@C

Na-promoted Co@C nanocomposites (denoted as Na-Co@C) were prepared by thermal decomposition of cobalt-sodium-ethylenediaminetetraacetate (Co-Na-EDTA) complexes at 450 °C (see Experimental section below) in H_2 atmosphere [27]. As shown in Fig. S1, the X-ray diffraction (XRD) pattern of this sample only shows the diffraction peaks corresponding to metallic cobalt, being *fcc* (PDF code: 96-900-8467) and *hcp* phases (PDF code: 96-900-8493) as the predominant and minor phases present, respectively. Moreover, the Raman spectrum (see Fig. S2) reveals that CoO_x species (Co_3O_4) are also detectable in the sample together with disordered carbon. To gain further understanding on the structure of Na-Co@C, the sample was studied by electron microscopy. As shown in Fig. 1a-b, Na-promoted Co@C nanocomposites consist of nanoparticles with sizes ranging from 15 to 150 nm (see Fig. S3 for more typical images and particle size distribution of the Na-Co@C sample). The high-resolution transmission electron microscopy (HRTEM) images in Fig. 1c and d show that Co nanoparticles are surrounded by thin carbon layers. Lattice fringes corresponding to metallic Co and Co_3O_4 can be observed in this sample, suggesting that, either part of the Co^{2+} species maintained their oxidation state, or part of the metallic Co was oxidized when exposed to air after the preparation. It is interesting to note that the core of the nanoparticles consisted of metallic cobalt, whereas Co_3O_4 patches are present on their surfaces below the carbon layers. Due to the presence of thin carbon layers, Co nanoparticles are protected from deep oxidation by air. Elemental mapping indicates that Co, C, O as well as Na are regularly dispersed in the nanocomposites (Fig. 1f–j). The Na-Co@C sample contains *ca.* 95 wt.% of Co and 2 wt.% of Na. An analogous Co@C sample free of Na has been also prepared (see the experimental section for synthesis procedure) [28]. Similar to the Na-promoted sample, HRTEM of the Co@C sample without Na shows the presence of Co nanoparticles surrounded by thin carbon layers (see Fig. S4), with CoO_x patches on the surface and
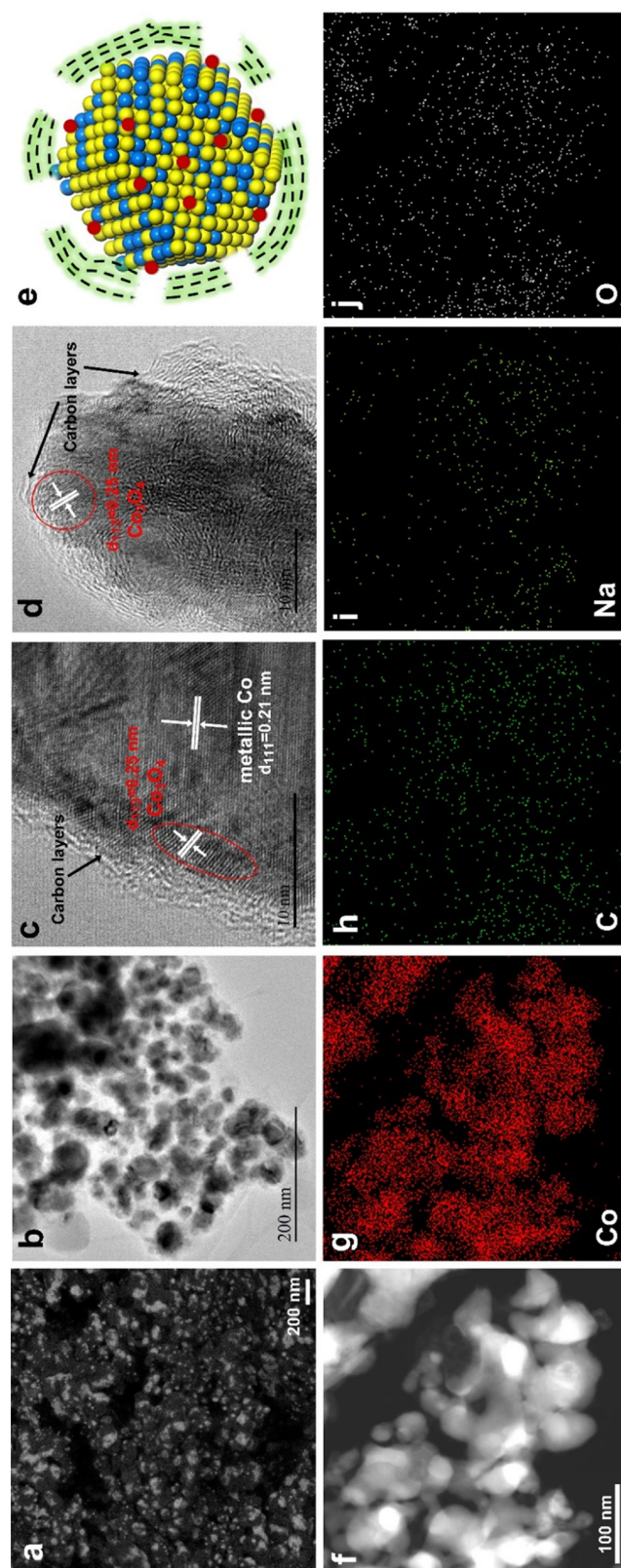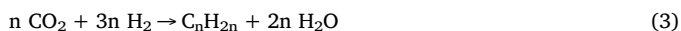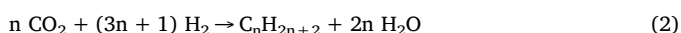

(caption on next page)

metallic Co as the core. The XRD pattern of the Co@C sample is also similar to Na-Co@C, showing the typical diffraction pattern of *fcc* metallic Co and a small proportion of *hcp* Co.

Fig. 1. Structural characterization of Na-Co@C sample. (a) Field-emission scanning electron microscopy (FESEM) image, (b) transmission electron microscopy (TEM) images, and (c, d) high-resolution transmission electron microscopy (HRTEM) images of Na-Co@C sample. (e) A schematic illustration of one Na-Co@C nanoparticle. Co, CoO$_x$ and sodium are represented by yellow, blue and red balls, respectively, while the carbon layers are represented as shaded dashed lines. (f) Scanning transmission electron microscopy (STEM) image and (g–j) corresponding elemental mapping of different elements in the Na-Co@C sample (For interpretation of the references to colour in this figure legend, the reader is referred to the web version of this article).

3.2. Photothermal hydrogenation of CO_2

The performance of three Co-based nanoparticulate catalysts for the photothermal hydrogenation of CO_2 under simulated sunlight is shown in Table 1. For comparison, the activity of commercial Co_3O_4 nanoparticles supplied by Sigma-Aldrich (the TEM images of commercial Co_3O_4 nanoparticles are shown in Fig. S5) and Co@C nanoparticles (without Na) was also measured under the same conditions. As can be seen (Table 1, entry 4), Co_3O_4 was able to catalyze the hydrogenation of CO_2, and CH_4 was the major product (> 98% selectivity). The formation of the hydrocarbons from CO_2 has been confirmed by ^{13}C labeling experiments. As shown in Figs. S6 and S7, products such as $^{13}CH_4$ and $^{13}C_3H_8$ coming from $^{13}CO_2$ are observed in mass spectrum, suggesting that the hydrogenation products in the catalytic tests indeed come from CO_2, not from the decomposition of carbon layers. In the case of Co@C catalyst, CH_4 also appeared as the dominant product and low selectivity to ethane (4.4%) was also observed. When Na-Co@C was used as the catalyst (Table 1, entry 1), CH_4 selectivity was markedly lower (62.7%), and more importantly, C2+ hydrocarbons and ethanol were also formed. These results suggest that the presence of Na is crucial for the production of C2+ hydrocarbons during the photothermal hydrogenation of CO_2, which is in line with classic heterogeneous catalytic systems favoring the formation of hydrocarbon chains [29].

The reaction equations of the reactions involved in the photo-assisted CO_2 hydrogenations are listed in Eqs. (1)–(3).

$$CO_2 + 4\,H_2 \rightarrow CH_4 + 2\,H_2O \tag{1}$$

$$n\,CO_2 + (3n+1)\,H_2 \rightarrow C_nH_{2n+2} + 2n\,H_2O \tag{2}$$

$$n\,CO_2 + 3n\,H_2 \rightarrow C_nH_{2n} + 2n\,H_2O \tag{3}$$

The oxidation half reaction in the CO_2 hydrogenation reaction should be the oxidation of H_2 to water. It is clear in the above reactions that, as in either $CO_2 + H_2$ or $CO + H_2$ to hydrocarbons, the ratio consumed H_2/CO_2 should be between 3 and 4 as a global situation. In our catalytic tests, the ratio of H_2/CO_2 in the feed gas is 5, which means H_2 is always excess. For instance, for the entry 1 in Table 1, H_2 conversion quantified by GC is 73.7%, corresponding to a H_2/CO_2 ratio of

~ 3.6, which is in line with the theoretical value.

We also tested Na-Co@C under thermal conditions without sunlight irradiation at the same temperature measured under photothermal conditions (235 °C). As shown in Table 1, the selectivity to C2+ hydrocarbons is lower than that obtained under photothermal conditions and a small amount of ethanol is also observed at high CO_2 conversion. The difference between the photothermal and thermal catalysis with Na-Co@C catalyst is more evident when the CO_2 conversion is below 40%. More C2+ hydrocarbons as well as ethanol are formed, suggesting that the light irradiation has significant influence on the product selectivity of Na-Co@C catalyst, which is different to previously reported works [13].

It has been claimed that solar light irradiation can increase the temperature of the catalyst surface, which further enhance the activity while does not influence the selectivity [12,13]. In our case, we have also tested the Na-Co@C catalyst for CO_2 hydrogenation under photothermal conditions at different temperature. As shown in Fig. S8, at similar CO_2 conversion (> 97%), the selectivity to C2+ hydrocarbons decreased with the temperature and more CH_4 was produced at higher temperature, suggesting that the improved selectivity to C2+ hydrocarbons is not caused by the thermal effects under the photothermal conditions.

Since various of products were observed on Na-Co@C sample under both photothermal and thermal conditions, the product distributions obtained at different CO_2 conversion were followed and given in Fig. 2. Under both photothermal and thermal conditions, the small amounts of CO formed initially were gradually consumed, and eventually could not be observed among the products (see Fig. 2a and b). This leads to conclude that CO was produced as a reaction intermediate, which then evolved towards the formation of higher hydrocarbons and alcohols through CO dissociation or a CO insertion mechanism respectively [30]. Notably, the selectivity to CO under photothermal conditions is slightly higher than under thermal conditions while selectivity to CH_4 is lower under photothermal conditions.

Furthermore, the variations of hydrocarbons and ethanol along the CO_2 hydrogenation were also followed. As presented in Fig. 2c, under photothermal conditions, the selectivity to ethanol and C2+ hydrocarbons is 6.5% and 36.3% respectively, when the CO_2 conversion is 37%. With the increase of CO_2 conversion, the selectivity to ethanol decreases, which could be caused by the photocatalytic reforming of ethanol with CO_2. According to the catalytic results, the chain growth probability factor (α) for hydrocarbon result in 0.55 at 37–58% CO_2 conversion and decreases to 0.38 at 97% CO_2 conversion.

It is clearly shown that, the yield of ethanol (< 0.8%) on Na-Co@C sample under thermal conditions is significantly lower than under photothermal process. Nevertheless, the selectivity to light olefins is also lower under thermal conditions (see Tables S1 and S2 in supporting formation). In the thermal process, the chain growth probability factor

Table 1
Photothermal and thermal CO_2 hydrogenation on different cobalt catalysts.

Sample	Conversion/%	Selectivity[c]/%								
		CH$_4$	CO	Ethanol	C2	C3	C4	C5	C6	Other products
Na-Co@C-photothermal[a]	97.0	62.7	–	0.6	16.5	12.5	4.8	2.0	0.6	0.3
Co@C-photothermal[a]	98.8	92.6	–	–	4.4	1.8	0.7	0.3	0.1	–
Na-Co@C-photothermal[a]	**37.0**	**50.2**	**4.8**	**6.5**	**13.0**	**12.7**	**5.2**	**3.3**	**2.0**	**2.3**
Co$_3$O$_4$-photothermal[a]	96.9	98.2	–	–	1.8	–	–	–	–	–
Na-Co@C-thermal[b]	91.5	67.4	–	0.4	11.9	10.4	5.1	2.7	1.3	0.6
Na-Co@C-thermal[b]	38.0	63.2	2.4	0.71	12.1	11.4	5.1	2.9	1.4	0.8

[a] Reaction conditions for photoassisted CO_2 hydrogenation reaction: mixture of CO_2 (20 mL), H_2 (100 mL), and N_2 (20 mL); catalyst mass, 75 mg; irradiation source, solar simulator. Blank controls in the absence of any solid catalyst or the reaction in the dark without heating did not lead to any product. The temperature of the sample (235 °C) under the photothermal conditions was measured by a thermocouple placed in close contact with the upper surface of the powdered solid.

[b] The thermal reaction was performed at the same temperature as the photothermal process without the presence of solar light irradiation.

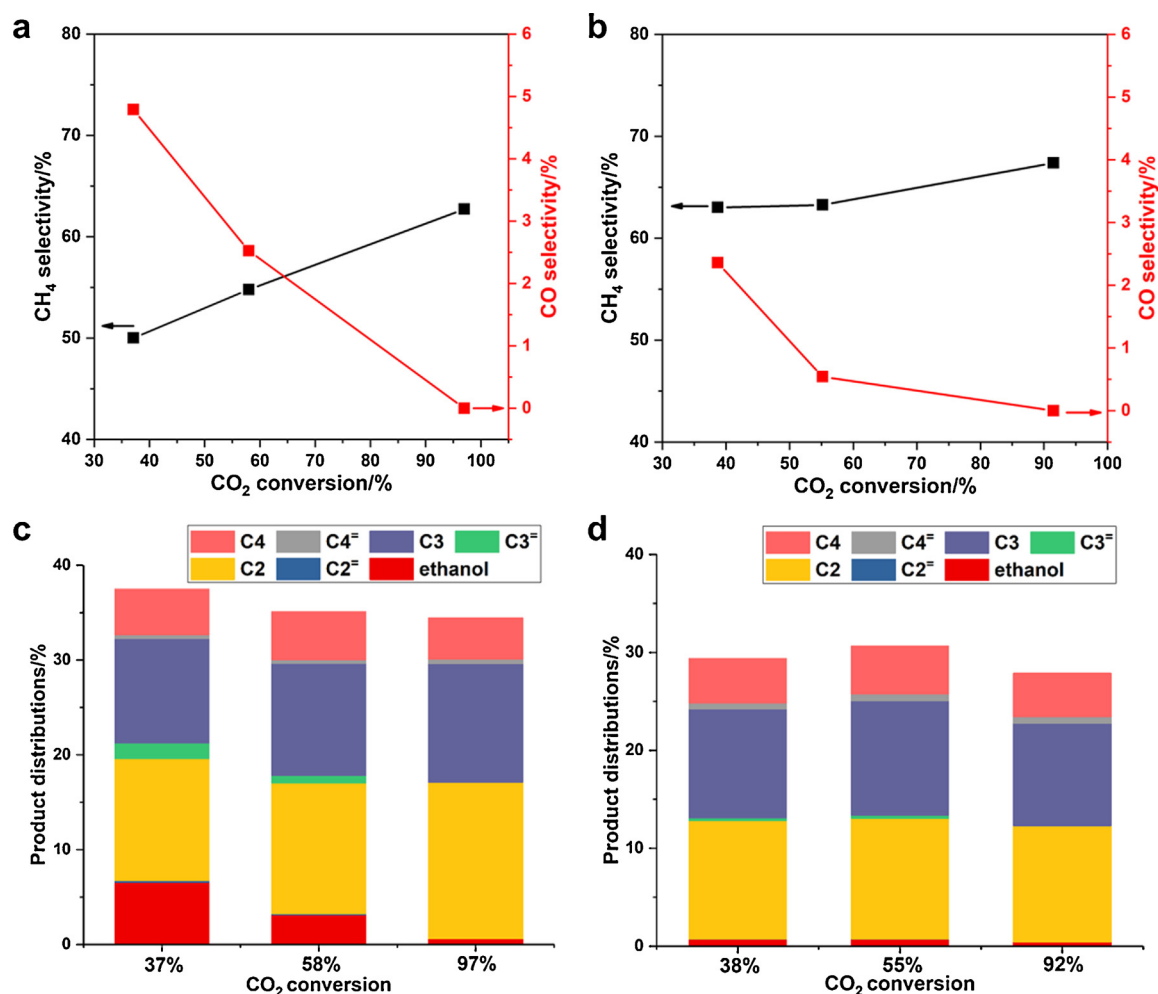[c] The selectivity to different products are normalized to carbon.

Fig. 2. Evolution of the products during CO_2 hydrogenation with Na-Co@C under photothermal and thermal conditions. (a) Selectivity to CH_4 and CO at different CO_2 conversion under photothermal conditions. (b) Selectivity to CH_4 and CO at different CO_2 conversion under thermal conditions. (c) Selectivity to C2+ hydrocarbons and ethanol under photothermal conditions at different CO_2 conversion. (d) Selectivity to C2+ hydrocarbons and ethanol under thermal conditions at different CO_2 conversion.

α is ~0.55 at all CO_2 conversion, which is similar to values reported in the literature for the CO_2 hydrogenation on cobalt-based catalysts [31]. The above catalytic results clearly indicate that, the solar light irradiation has significant influences on the product distribution during CO_2 hydrogenation. With the help of sunlight irradiation, the selectivity to C2+ hydrocarbons and ethanol is promoted, especially at medium CO_2 conversion (< 50%).

3.3. Effect of light on the catalytic performance

In previous works, it has been reported that CO_2 hydrogenation can be enhanced under solar light irradiation [12,32]. Herein, we have also observed that the initial reaction rate of the CO_2 hydrogenation on Na-Co@C under thermal conditions was lower than for the analogous process performed under simultaneous irradiation and external heating conditions (see Fig. S9). The Na-Co@C nanomaterials show an intense light absorption profile throughout the entire UV–vis spectrum (see Fig. S10). In order to investigate on which wavelengths might be responsible for the activation of CO_2 hydrogenation, irradiations were performed using monochromatic light of selected frequencies (see Fig. S11). Light in the UV range (< 400 nm) was observed to promote the reaction in a noticeable way [33]. Therefore, it can be deduced that photo-generation of charges (electron-hole pairs) on Co@C nanoparticles may participate in the CO_2 hydrogenation reaction. A recent study on the use of carbon-coated iron nanoparticles in a similar process

suggested that hot electrons generated by absorption of UV light were responsible for activating CO_2 [12].

In the present system, we considered the hypothesis of direct participation of the photo-generated charges, which would be transferred to appropriate adsorbed species and then involved in CO_2 hydrogenation reaction. Therefore, control experiments by adding a hole scavenger in the reaction system were designed to check whether consumption of photo-generated charges had any effect on activity. A series of sunlight-assisted experiments in the absence or in the presence of methanol as a hole scavenger were performed (see Fig. S12). The introduction of a small amount of methanol vapor in the cell leads to a slight decrease in the initial reaction rates. A further increase in the amount of methanol leads to a significantly greater decrease of the initial activity. Based on the aforementioned evidences, it is proposed here that the photothermal CO_2 hydrogenation on Na-Co@C nanocomposites is to some extent activated by the UV light.

4. Mechanistic studies based on in situ spectroscopy

Due to the complexity of the CO_2 hydrogenation reaction, characterizations of the catalyst under working conditions at molecular level have been carried out to identify the nature of active sites and establish correlations between structure and catalytic reactivity. Thus, near-ambient pressure X-ray photoelectron spectroscopy (AP-XPS) and in situ Raman studies have been performed providing useful

information on the nature of surface intermediate species involved in the reaction mechanism and the chemical states of the catalyst surface in the presence of CO_2/H_2 mixture. A detailed analysis of surface species under reaction conditions will allow to shed light on the role of light irradiation and the promoting effect of sodium on the catalytic behavior of Na-Co@C sample for CO_2 hydrogenation.

4.1. AP-XPS studies on the surface properties of Co-based catalysts

In contrast to the Na-Co@C sample, a different catalytic behavior has been observed on the Na-free Co@C sample under photoassisted reaction conditions (see Table 1). The role of sodium in FTS cobalt based catalysts has extensively been discussed in the literature. It has been proposed that sodium can stabilize cobalt carbide species which serve as active sites for the formation of oxygenates [34,35]. In some other works, it is suggested that cobalt carbides can suppress the hydrogenation of C=C bonds and facilitate the desorption of olefins, leading to higher selectivity to olefins [36]. However, it has also been proposed that cobalt carbides can decrease the reducibility of cobalt oxide and/or block active sites, resulting in lower catalytic activity for FTS [37,38].

As shown in Fig. 3a, carbide species have been detected on the Na-Co@C sample in the $Co2p_{3/2}$ spectra under light irradiation. At the reaction temperature (250 °C), Co2p3/2 peak fitting shows the co-existence of Co° (9%), CoO (88%) and Co_2C (3%) species. Notably, the formation of carbide species is rather low, leading us to question their

participation in the formation of alcohols under our reaction conditions. The low reducibility of cobalt species under reaction conditions should also be noted. On the other hand, under light irradiation and in the absence of Na, Co2p3/2 peak fitting shows the presence of Co° (9%), CoO (79%) and Co_2C (12%) at 250 °C (Fig. 3b). A higher amount of cobalt carbide is observed on the Co@C sample while the amount of metallic Co is similar to Na-Co@C sample, implying that the promotion effect of Na does not seem to relate with either the increase of reducibility or stabilization of carbide. Nevertheless, the $Co2p_{3/2}$ peak fitting of the Na-Co@C sample under thermal condition (see Fig. 3c) shows the presence of Co° (15%), CoO (72%) and Co_2C (13%), suggesting that sunlight irradiation can suppress the formation of cobalt carbide.

The abovementioned XPS results of $Co2p_{3/2}$ region indicate that, higher selectivity to C2+ hydrocarbons and ethanol on Na-Co@C sample under photothermal conditions is probably not related with cobalt carbide species. Moreover, considering the similar percentage of metallic Co in the above three cases, it seems that the observed different catalytic behavior is not related with the reducibility of the Co catalyst.

4.2. AP-XPS studies on the surface carbon species

Though several reaction paths have been proposed for the CO_2 hydrogenation reaction, the starting point is the activated $CO_2^{\delta-}$ specie which can either dissociate into CO + O or undergo direct hydrogenation [39]. The in situ formed CO can be further hydrogenated or
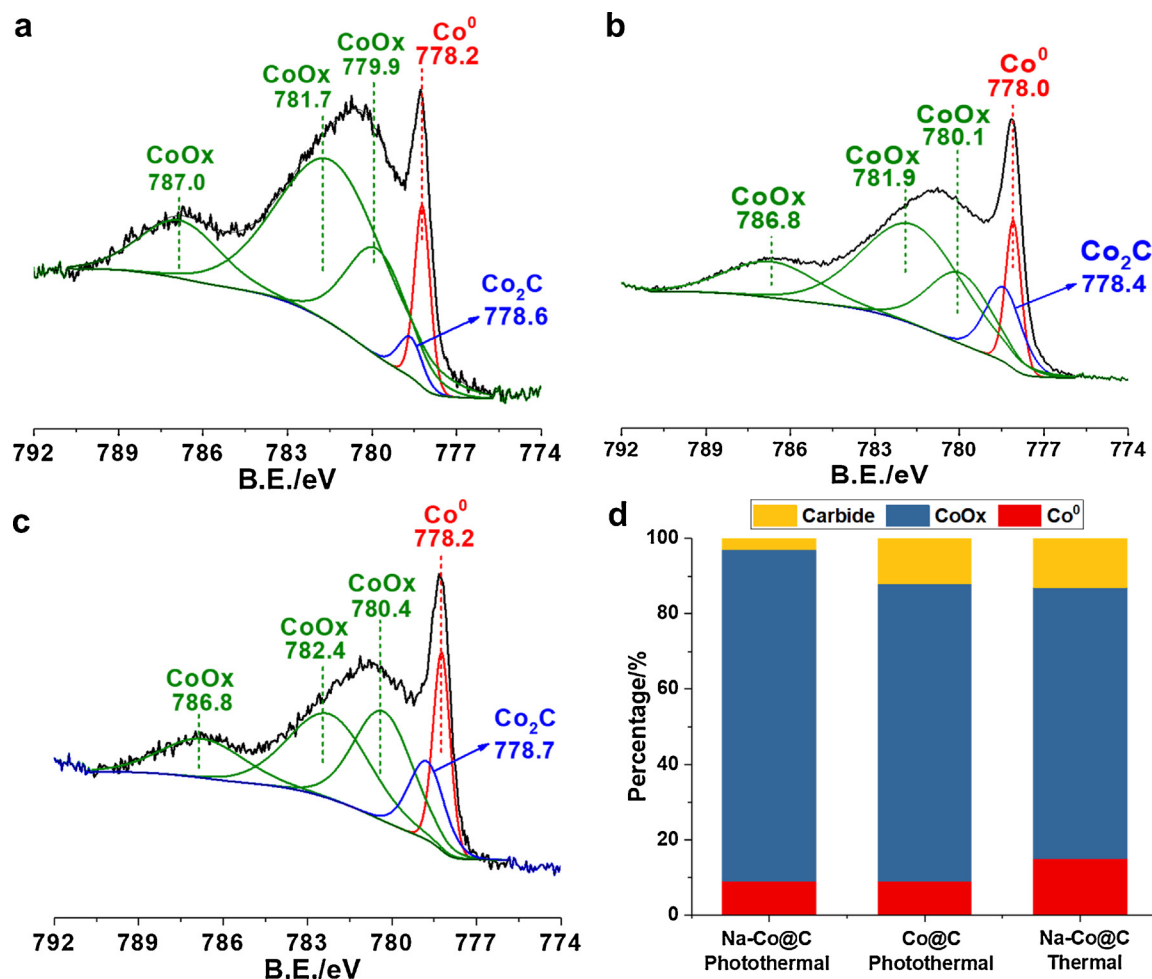
Fig. 3. AP-XPS spectra of $Co2p_{3/2}$ region obtained at 250 °C with incident X-ray energy of 1000 eV. (a) Na-Co@C under photothermal conditions, (b) Co@C under photothermal conditions and (c) Na-Co@C under thermal conditions. (d) Percentage of cobalt carbide, CoOx and metallic Co° in different Co-based catalysts based on the AP-XPS spectra.
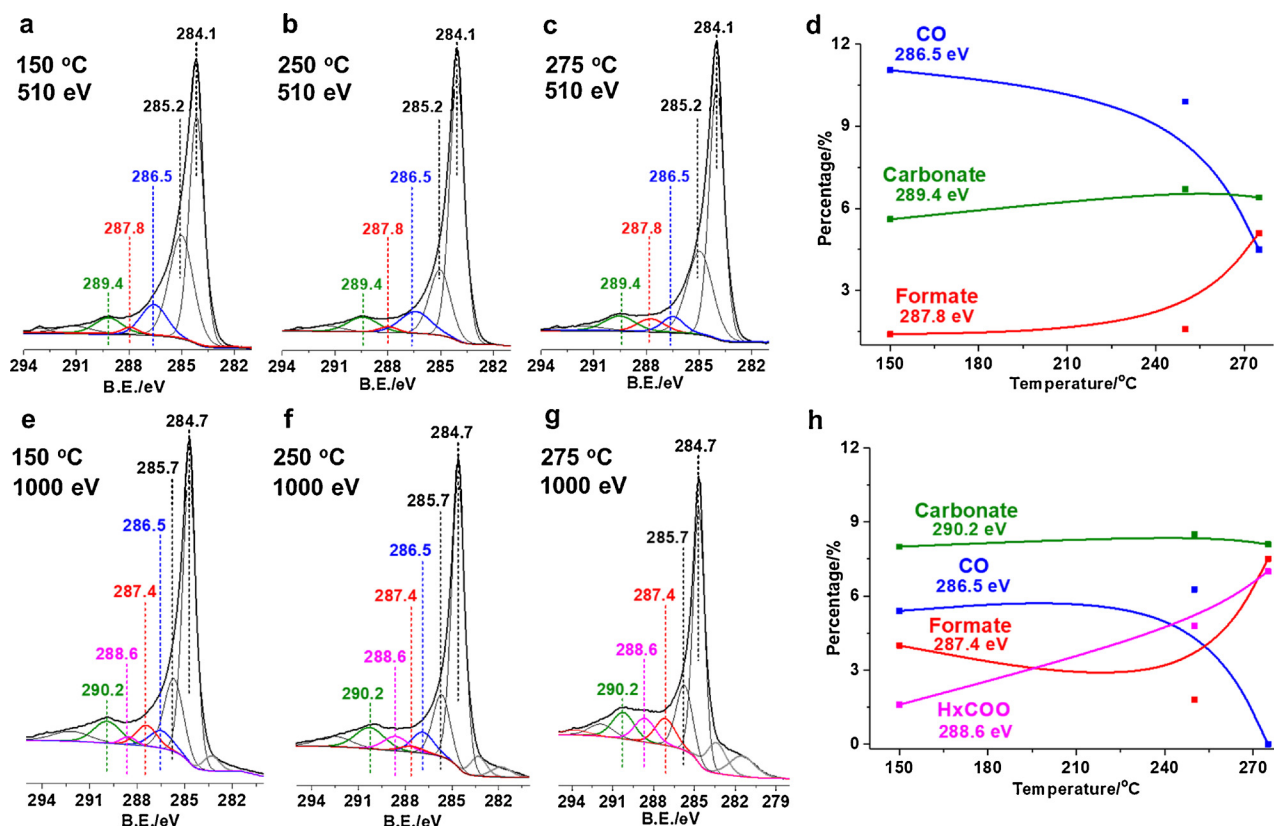
Fig. 4. Ambient-pressure XPS spectra of Na-Co@C sample during CO_2 hydrogenation reaction conditions ($P_{CO_2} = 0.1$ mbar and $P_{H_2} = 0.5$ mbar) under photothermal conditions. (a–c) C1s spectra obtained with incident X-ray energy of $h\nu = 510$ eV. (d) Percentage of different types of carbon species at different temperature according to the spectra obtained at $h\nu = 510$ eV. (e–g) Spectra obtained with incident X-ray energy of $h\nu = 1000$ eV. (h) Percentage of different types of carbon species at different temperature according to the spectra obtained at $h\nu = 1000$ eV.

dissociate into C and O ad-atoms, resulting in the formation of different surface species, like for instance formyl (HCO), hydroxycarbene (HCOH), hydroxymethyl (H_2COH), methyl (CH_3), methylene (CH_2), methylidyne (CH) and hydroxymethylidyne (COH). Chain growth takes place by a surface polymerization condensation reaction process resulting in the formation of paraffins, olefins and oxygenates. The types of the surface carbon species can be used as fingerprint for reaction pathways towards different products. Therefore, we firstly have studied the surface carbon species by AP-XPS to follow their evolution on Co-based catalysts.

The C1s core levels of the Na-Co@C and Co@C samples in presence

of CO_2 and H_2, under thermal and photothermal reaction conditions, are shown in Figs. 4–6, where XPS spectra have been acquired at two photon energies, $h\nu = 510$ eV and $h\nu = 1000$ eV, in order to analyze at different depths of the sample. Firstly, the Na-Co@C sample has been studied. Two C1s peaks at BE 285.2–285.6 and 284.1–284.7 eV have been observed in the Na-Co@C sample under light irradiation, corresponding to carbon layers covered on Co nanoparticles. Moreover, the C1s spectra (Fig. 4a-c) under light irradiation and working at $h\nu = 510$ eV, show predominately CO (BE 286.5 eV) as main component in addition to formate (BE 287.8 eV) and carbonate species (BE 289.4 eV) [40–42]. When working at higher photon energy (1000 eV)
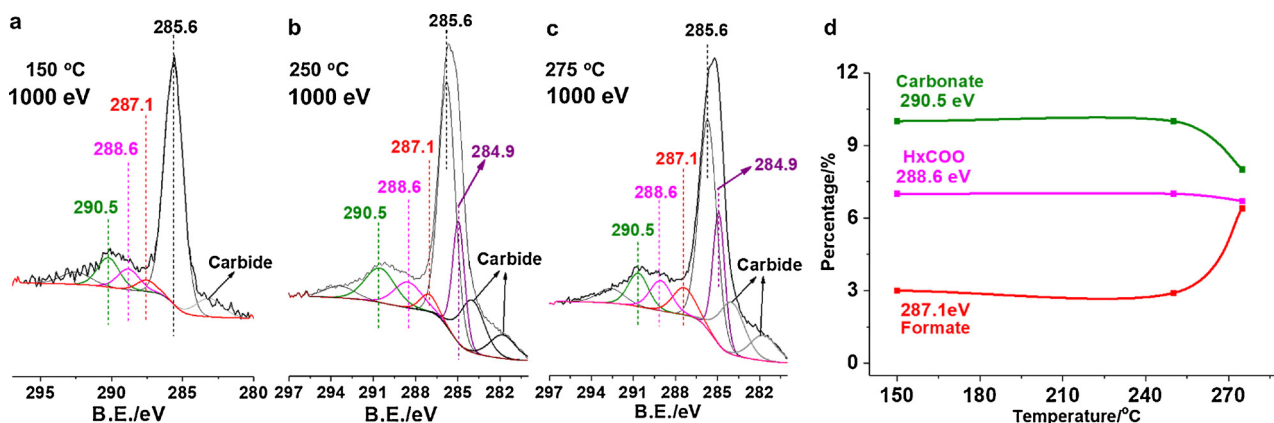

Fig. 5. Ambient-pressure XPS spectra of Na-Co@C sample during CO_2 hydrogenation reaction conditions ($P_{CO_2} = 0.1$ mbar and $P_{H_2} = 0.5$ mbar) under thermal conditions. (a–c) C1s AP-XPS spectra of Na-Co@C sample under thermal conditions obtained with incident X-ray energy of $h\nu = 1000$ eV. (d) Percentage of different types of carbon species at different temperature according to the spectra obtained at $h\nu = 1000$ eV.
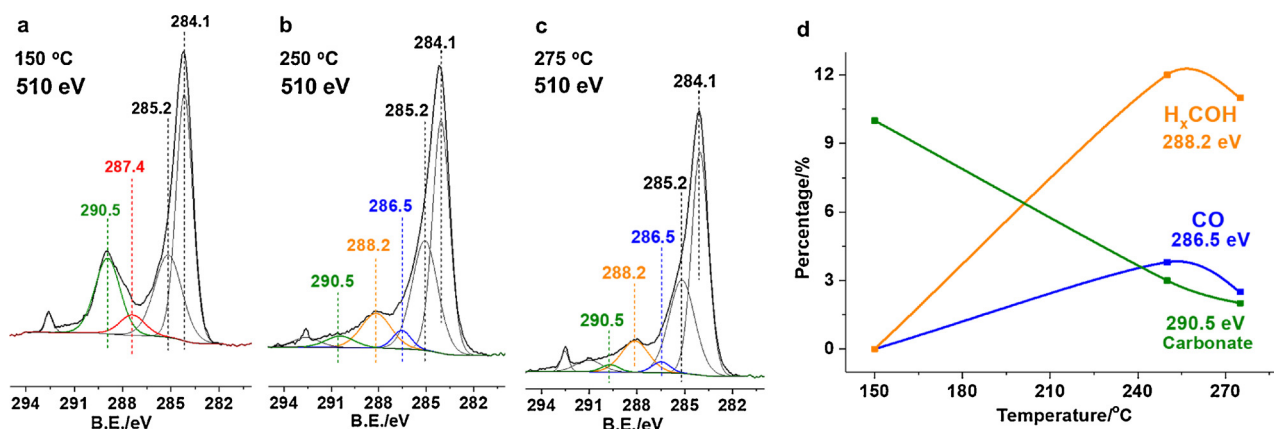
Fig. 6. Ambient–pressure XPS spectra of Co@C sample during CO_2 hydrogenation reaction conditions (P_{CO_2} = 0.1 mbar and P_{H_2} = 0.5 mbar) under photothermal conditions. (a–c) C1s AP-XPS spectra of Co@C sample under photothermal conditions obtained with incident X-ray energy of hv = 510 eV. (d) Percentage of different types of carbon species at different temperature according to the spectra obtained at hv = 510 eV.

(Fig. 4e–g), besides CO (BE 286.5 eV), formate (BE 287.4 eV) and carbonate species (BE 290.2 eV), an additional component at 288.6 eV is observed. In the O1s region (Fig. S13a), a new component at 532.8 eV appears when increasing the reaction temperature, showing similar behavior to the C1s component at BE 288.6 eV. Based on the high BE of both species and their parallel growing, we can tentatively assign both components to some type of hydrogen-carbonate intermediate specie, i.e H_xCOO^*. Peak areas of each component according to the fitting results of C1s spectra, and their evolution as a function of the temperature, are given in Fig. 4d and h. Taking into consideration that CO is predominantly observed at low photon energy (being high surface sensitive conditions) and Co nanoparticles are covered by thin carbon layers, the XPS results indicate that CO is stabilized on the surface carbon layers of the Na-Co@C sample. At higher photon energy (hv = 1000 eV), the contribution of formate and H_xCOO^* in the C1s peak increases, indicating their stronger interaction with Co surface covered by the carbon layers. Based on Fig. 4d and h, it can be observed that when increasing reaction temperature, the signal intensity of the surface CO decreases, while formate species and H_xCOO^* increase. Meanwhile carbonate like species remains practically stable with the temperature. This behavior indicates that CO, formate and H_xCOO^* behave as intermediate species while carbonate species, stabilized either on cobalt surface or on the carbon layer, are not involved in the reaction pathways.

The CO_2 hydrogenation on Na-Co@C sample under thermal conditions has also been studied by AP-XPS. As shown in Table 1 and Fig. 2, the product distribution under thermal conditions with Na-Co@C for CO_2 hydrogenation is similar to the situation under photothermal conditions, although selectivity to C2 + hydrocarbons and ethanol were lower under thermal conditions. Based on the AP-XPS studies (Fig. 5a–c), CO (BE 286.7 eV) is not detected on the catalyst surface under thermal conditions, while it is detected in the gas phase (Fig. S14), suggesting that CO interacts weakly with the catalyst surface under thermal conditions. Since the stabilization of CO on catalyst surface is a key for the formation of oxygenates during CO_2 hydrogenation, the absence of CO on Na-Co@C under thermal conditions can explain its low selectivity to ethanol. Besides, carbonate (BE 290.5 eV), formate (BE 287.1 eV) and H_xCOO^* (BE 288.6 eV), are also predominantly observed in the C1s spectra. Notoriously carbide species with BE 283.7 and 281.6 eV (also observed in the Na-Co@C sample under light irradiation) and graphitic carbon species and/or CHx species with BE at 284.9 eV are also detected, which is in line with the higher amount of cobalt carbide as observed in Fig. 3 for the Na-Co@C sample under thermal conditions. This difference implies that the sunlight irradiation can suppress the deposition of carbon on cobalt.

Considering our previous hypothesis where UV light plays an important role in the CO_2 activation through the formation of electron hole pairs, a support for this hypothesis can be found from the AP-XPS studies. As we have mentioned before, two C1s peaks at BE 285.2–285.6 and BE 284.1-284.7 eV have been observed in the Na-Co@C sample under light irradiation (Fig. 4). The first ones corresponding to carbon are also observed in the Na-Co@C sample without sunlight irradiation (Fig. 5), while the later ones are only observed on irradiated samples. The low BE of the C1s peak at BE 284.1–284.7 eV may account for electron-rich carbon species from the carbon layer formed under light irradiation, which can play an important role in the activation of CO_2 to $CO_2^{\delta-}$, enhancing the CO_2 dissociation to CO and O. These results can explain the higher initial reaction rate for CO_2 hydrogenation on Na-Co@C sample under sunlight irradiation.

In order to explain the ∼ 92% CH_4 selectivity observed in the Co@C catalyst, and in an attempt to find out why and how Na plays an effect of the product distribution, the evolution of carbon intermediate species at different reaction temperatures has been followed by AP-XPS studies (Fig. 6). Surprisingly, a different reaction intermediate is observed in the non-promoted Co@C catalyst, where a new component at BE 288.2 eV, not observed in the Na-Co@C sample, is predominant. In addition, CO (BE 286.5 eV) is also formed together with surface carbonate species (BE 290.5 eV). Formate species (BE 287.4 eV) are only detected at low temperature (Fig. 6a–c). Based on the growth of a parallel new component at BE 530.6 eV in the O1s peak (Fig. S13b), associated to hydroxyl groups, we can assign the peak at BE 288.2 eV to enol like species (H_xCOH). These enol like species are unstable on Co surface, and further C−OH scission would lead to formation of CH_x species, which can be further hydrogenated into CH_4, as detected in the catalytic studies.

Combining the above AP-XPS results, it can be concluded that, under light irradiation, the promoting effect of sodium on the production of C2 + hydrocarbons and oxygenate cannot be ascribed to any of the effects described previously in the literature [43–45]. The effect of Na in our system is probably related with the modulation of the surface intermediates during the catalytic process of CO_2 hydrogenation, resulting in different product distributions. Meanwhile, we have observed that light plays an important role in the reaction mechanism, by modulating the types of intermediates species and their stability (especially CO) on the surface of Co nanoparticles.

4.3. In situ Raman studies on the surface carbon species

The formation of carbon species in the CO_2 hydrogenation process, already detected in the AP-XPS studies, has also been analyzed by operando Raman studies. As shown before in Fig. 3, the amount of cobalt carbide formed on Na-Co@C under thermal conditions is more than
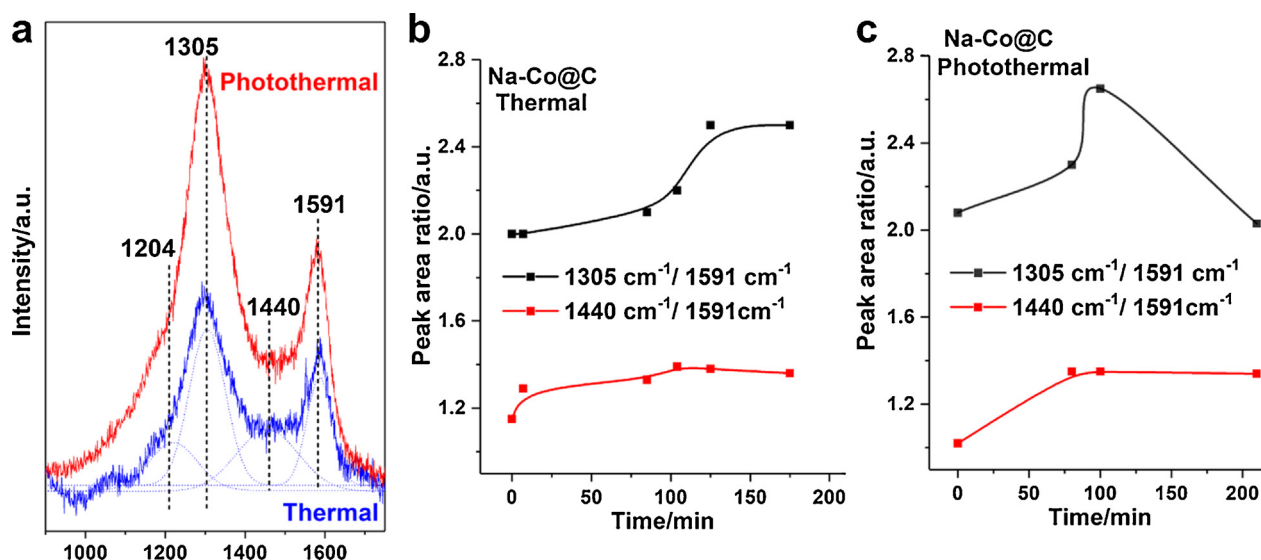
Fig. 7. In situ Raman spectra of Na-Co@C under thermal and photothermal conditions for CO_2 hydrogenation. (a) Raman spectra obtained with Na-Co@C sample after 100 min reaction under photothermal (red curve) and thermal (blue curve) conditions for CO_2 hydrogenation. (b) Peak area ratio of the Raman bands at different reaction time under photothermal and thermal conditions for CO_2 hydrogenation (For interpretation of the references to colour in this figure legend, the reader is referred to the web version of this article).

under photothermal conditions. The high sensitivity of Raman spectroscopy to carbonaceous species, and the possibility to work under more realistic reaction conditions (1 bar in Raman versus 0.6 mbar in AP-XPS) enables us to obtain more realistic information about the formation of carbon species and their evolution under operando conditions.

Peak fitting of the Raman spectra of the Na-Co@C catalyst, shows several bands at 1204, 1305, 1440 and 1591 cm^{-1} associated to different carbon species (see Fig. 7), which can be ascribed to disordered graphite, capillary carbon or defects in graphite, amorphous carbon and graphite like carbon, respectively [46,47]. Under thermal CO_2 hydrogenation conditions, an increase in the amount of amorphous carbon (1.15 to 1.39) and capillary carbon (2.08 to 2.5) is observed with reaction time. Under photothermal conditions, the amount of capillary carbon species increases in the first 100 min from 2.08 to 2.65 and then decreases to 2.03, while amorphous carbon increases and remains practically constant (1.02 to 1.35). Thus, the in situ Raman results infer that sunlight irradiation can suppress the carbon deposition on Na-Co@C catalyst. Such effect may cause the low percentage of cobalt carbide formed on the Na-Co@C catalyst under photothermal conditions.

5. Influence of sunlight irradiation on the structure of the Co-based catalysts

The morphologies of Co-based catalysts after CO_2 hydrogenation reactions under thermal and photothermal conditions have been studied by TEM. As shown in Fig. S15 the morphology of Na-Co@C after photothermal CO_2 hydrogenation is different to the pristine sample. Rod-like structures are formed along the spherical Co nanoparticles. Elemental mapping (see Fig. S16) results show that, those rod-like structures contains Co, suggesting that structural reconstruction occurred during the CO_2 hydrogenation reaction under photothermal conditions. Furthermore, HRTEM images indicate that, those rod-like structures corresponding to Co_3O_4. However, those Co_3O_4 species may come from the re-oxidation of metallic Co° or Co_2C species after contact with air during preparation of the samples for TEM measurements. Besides, we have also measured the other Co catalysts after CO_2 hydrogenation reactions. As shown in Figs. S17–S19, rod-like structures can be observed in all the cases, suggesting the structural reconstruction

is a common phenomenon in Co catalysts for CO_2 hydrogenation reaction [48]. Catalyst reconstruction could be also reflected from the AP-XPS data where the number of exposed cobalt surface sites increases under reaction conditions (Table S3). It should be noted that, the size of the rod like structures formed in Co_3O_4 nanoparticles are larger than those formed in either Na-Co@C or Co@C, which may be related with the absence of carbon layers on the Co nanoparticles.

In addition, in conventional Fischer-Tropsch processes, the presence of the Co° **hcp** phase plays an important role during the growth of carbon chain for producing higher hydrocarbons [49–51]. As shown in Fig. S20, the percentage of the Co° **hcp** phase increases significantly in the Na-Co@C sample after the photothermal reaction. For comparison purposes, the XRD pattern of the Na-Co@C sample after only-thermal catalytic hydrogenation of CO_2 was also measured. The percentage of **hcp** phase Co also increased in this case, but not as much as after the photothermal reaction, implying that solar light irradiation during the CO_2 hydrogenation reaction can promote the transformation of Co species into the **hcp** phase, which may have influence on the catalytic behavior [49–51].

As shown in Fig. S21, excellent activity and high selectivity towards C2 and C3 hydrocarbons was observed during the first reuse of the catalyst. However, significant deactivation of the catalyst became apparent during the second reuse. It should be noted that, the catalyst was always kept in reductive atmosphere during the first and second reuse. According to the spectroscopic characterizations in this work and the literature, it seems that, the formation of cobalt carbide or graphitic carbon on the catalyst surface may contribute to the loss of activity [52,53]. Since cobalt carbide can be oxidized by air, then the blocked surface sites by cobalt carbide or graphitic carbon can be recovered after mild oxidation treatment. In fact, after exposing the reused catalyst to air at ambient temperature and pressure, the high activity and selectivity of Na-Co@C was again recovered (see Fig. S21).

6. Proposed reaction mechanism

Based on the above spectroscopic studies, we can conclude that light irradiation plays an important role in the CO_2 activation mechanism (as shown in Fig. 8), favoring the RWGS reaction ($CO_2 + H_2 \rightarrow CO + H_2O$) and the stabilization of CO on the catalyst surface. The direct role of light has been ascribed to an electronic effect where electrons generated
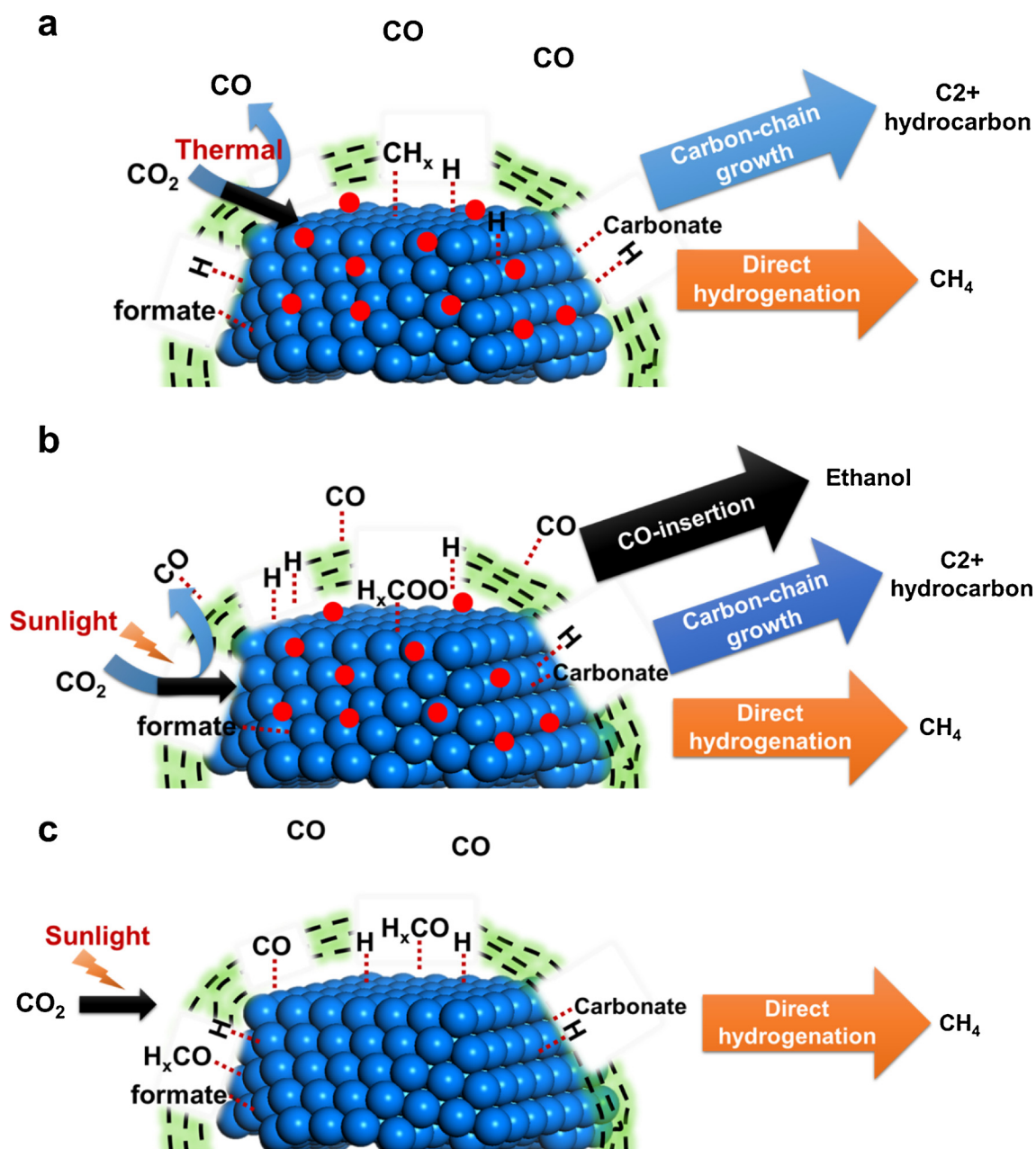
Fig. 8. Schematic illustration of the CO_2 hydrogenation on Na-Co@C and Co@C catalysts under thermal and photothermal conditions. Sodium is shown with red circles. (a) Under thermal conditions, Na-Co@C catalyst mainly produce CH_4 and C2+ hydrocarbons. (b) Under photothermal conditions, ethanol is also produced as well as C2+ hydrocarbon and CH_4. (c) Under photothermal conditions, CH_4 is the predominant product on Co@C sample, due to the fast hydrogenation of the intermediates instead of C−C coupling reaction (For interpretation of the references to colour in this figure legend, the reader is referred to the web version of this article).

by absorption of UV light are responsible for activating CO_2 to $CO_2^{\delta-}$, promoting CO_2 dissociation into CO, and the stabilization of CO on the catalyst surface. The stabilization of CO contributes to a higher selectivity toward ethanol by a CO insertion mechanism. Moreover, a clear effect of light on the chain growth process can also be deduced according to the different surface intermediates observed by AP-XPS. This can be reflected from the catalytic results where under light irradiation the ASF hydrocarbon distribution differs from the thermal process, with a higher selectivity to C_2H_6 and C_3H_8 and ethanol. The higher selectivity to C_2H_6 and C_3H_8 under light irradiation can be related to a lower concentration of surface C species, or to low metal-C adsorption strength promoting hydrocarbon desorption. At this point, and based on our spectroscopic data, it has been observed that sunlight irradiation can reduce the metal-carbon interaction. Indeed, the

amount of carbide species observed in the AP-XPS spectra is markedly lower in the presence of light than under thermal conditions. Nevertheless, we have also observed the influence of light irradiation on the phase structure of Co catalysts, which show higher amount of Co **hcp** phase under sunlight irradiation. Finally, and in agreement to literature data, sodium plays an important role on the C−C formation by influencing the nature of intermediate species on the catalyst surface. In the absence of sodium (Fig. 8c), enol species seem to be stabilized, and the C−OH scission favors the formation of CH_4.

7. Conclusions

In summary, we report the application of Na-Co@C nanocomposites for photocatalytic hydrogenation of CO_2 to C2+ hydrocarbons and

ethanol. Under photothermal conditions the Na-promoted Co@C sample shows almost 100% selectivity to hydrocarbons as well as high selectivity to C2 and C3 products (16.5% and 12.5% respectively) at > 97% CO_2 conversion. Photo-generation of charges on Co@C nanoparticles upon UV light absorption, in addition to the favored formation of active ***hcp*** phases under such conditions, proved the activating role of sunlight irradiation in the photothermal process. Control experiments confirm the participation of photo-generated charges in the catalytic process. In addition, AP-XPS studies have shown a direct role of light irradiation on the formation of electron rich carbon species on the surface of Na-Co@C nanoparticles. These species are involved in CO_2 activation to $CO_2^{\delta-}$, promoting CO_2 dissociation into CO. Moreover, CO is stabilized by interaction with the carbon layers on the catalyst surface, enabling the formation of ethanol via a CO insertion mechanism. Based on spectroscopic studies, this work shows how the light irradiation can influence the surface intermediate species during CO_2 hydrogenation reaction, leading to different reaction pathways.

Acknowledgements

Appendix A. Supplementary data

Supplementary material related to this article can be found, in the online version, at doi:https://doi.org/10.1016/j.apcatb.2018.04.060.

References

[1] G.A. Ozin, Adv. Mater. 27 (2015) 1957–1963.
[2] N.S. Lewis, D.G. Nocera, Proc. Natl. Acad. Sci. U. S. A. 103 (2006) 15729–15735.
[3] D.G. Nocera, Acc. Chem. Res. 45 (2012) 767–776.
[4] L. Liu, F. Gao, H. Zhao, Y. Li, Appl. Catal. B Environ. 134-135 (2013) 349–358.
[5] Z. Sun, J.M.T.A. Fischer, Q. Li, J. Hu, Q. Tang, H. Wang, Z. Wu, M. Hankel, D.J. Searles, L. Wang, Appl. Catal. B Environ. 216 (2017) 146–155.
[6] S.N. Habisreutinger, L. Schmidt-Mende, J.K. Stolarczyk, Angew. Chem. Int. Ed. 52 (2013) 7372–7408.
[7] A. Corma, H. Garcia, J. Catal. 308 (2013) 168–175.
[8] F. Sastre, A.V. Puga, L. Liu, A. Corma, H. Garcia, J. Am. Chem. Soc. 136 (2014) 6798–6801.
[9] A.V. Puga, Top. Catal. 59 (2016) 1268–1278.
[10] X. Meng, T. Wang, L. Liu, S. Ouyang, P. Li, H. Hu, T. Kako, H. Iwai, A. Tanaka, J. Ye, Angew. Chem. Int. Ed. 126 (2014) 11662–11666.
[11] W. Sun, C. Qian, L. He, K.K. Ghuman, A.P. Wong, J. Jia, A.A. Jelle, P.G. O'Brien, L.M. Reyes, T.E. Wood, A.S. Helmy, C.A. Mims, C.V. Singh, G.A. Ozin, Nat. Commun. 7 (2016) 12553.
[12] H. Zhang, T. Wang, J. Wang, H. Liu, T.D. Dao, M. Li, G. Liu, X. Meng, K. Chang, L. Shi, T. Nagao, J. Ye, Adv. Mater. 28 (2016) 3703–3710.
[13] G. Chen, R. Gao, Y. Zhao, Z. Li, G.I.N. Waterhouse, R. Shi, J. Zhao, M. Zhang, L. Shang, G. Sheng, X. Zhang, X. Wen, L.Z. Wu, C.H. Tung, T. Zhang, Adv. Mater. 30 (2018), http://dx.doi.org/10.1002/adma.201704663.
[14] P. Lanzafame, S. Abate, C. Ampelli, C. Genovese, R. Passalacqua, G. Centi, S. Perathoner, ChemSusChem 10 (2017) 4409–4419.
[15] A. Navarrete, G. Centi, A. Bogaerts, Á. Martín, A. York, G.D. Stefanidis, Energy Technol. 5 (2017) 796–811.
[16] R.W. Dorner, D.R. Hardy, F.W. Williams, H.D. Willauer, Energy Environ. Sci. 3 (2010) 884.
[17] M.D. Porosoff, B. Yan, J.G. Chen, Energy Environ. Sci. 9 (2016) 62–73.
[18] G. Centi, E.A. Quadrelli, S. Perathoner, Energy Environ. Sci. 6 (2013) 1711.
[19] A.Y. Khodakov, W. Chu, P. Fongarland, Chem. Rev. 107 (2007) 1692–1744.
[20] W. Wang, S. Wang, X. Ma, J. Gong, Chem. Soc. Rev. 40 (2011) 3703–3727.
[21] V. Iablokov, S.K. Beaumont, S. Alayoglu, V.V. Pushkarev, S. Specht, J. Gao, A.P. Alivisatos, N. Kruse, G.A. Somorjai, Nano Lett. 12 (2012) 3091–3096.
[22] M.P. Andersson, F. Abild-Pedersen, I.N. Remediakis, T. Bligaard, G. Jones, J. Engbæk, O. Lytken, S. Horch, J.H. Nielsen, J. Sehested, J. Catal. 255 (2008) 6–19.
[23] J. Gao, Q. Liu, F. Gu, B. Liu, Z. Zhong, F. Su, RSC Adv. 5 (2015) 22759–22776.
[24] A.Y. Khodakov, W. Chu, P. Fongarland, Chem. Rev. 107 (2007) 1692–1744.
[25] Y. Zhao, B. Zhao, J. Liu, G. Chen, R. Gao, S. Yao, M. Li, Q. Zhang, L. Gu, J. Xie, X. Wen, L.Z. Wu, C.H. Tung, D. Ma, T. Zhang, Angew. Chem. Int. Ed. 55 (2016) 4215–4219.
[26] V. Pérez-Dieste, L. Aballe, S. Ferrer, J. Nicolàs, C. Escudero, A. Milán, E. Pellegrin, J. Phys. Conf. Ser. 425 (2013) 072023.
[27] L. Liu, P. Concepción, A. Corma, J. Catal. 340 (2016) 1–9.
[28] L. Liu, F. Gao, P. Concepción, A. Corma, J. Catal. 350 (2017) 218–225.
[29] T. Riedel, M. Claeys, H. Schulz, G. Schaub, S.-S. Nam, K.-W. Jun, M.-J. Choi, G. Kishan, K.-W. Lee, Appl. Catal. A Gen. 186 (1999) 201–213.
[30] M. Ojeda, R. Nabar, A.U. Nilekar, A. Ishikawa, M. Mavrikakis, E. Iglesia, J. Catal. 272 (2010) 287–297.
[31] C.G. Visconti, M. Martinelli, L. Falbo, L. Fratalocchi, L. Lietti, Catal. Today 277 (2016) 161–170.
[32] J. Jia, H. Wang, Z. Lu, P.G. O'Brien, P. Ghoussoub, P. Duchesne, Z. Zheng, P. Li, Q. Qiao, L. Wang, A. Gu, A.A. Jelle, Y. Dong, Q. Wang, K.K. Ghuman, T. Wood, C. Qian, Y. Shao, C. Qiu, M. Ye, Y. Zhu, Z.H. Lu, P. Zhang, A.S. Helmy, C.V. Singh, N.P. Kherani, D.D. Perovic, G.A. Ozin, Adv. Sci. 4 (2017) 1700252.
[33] G. Simon, L. Meziane, A. Courty, P. Colomban, I. Lisiecki, J. Raman Spectrosc. 47 (2016) 248–251.
[34] X. Deng, A. Verdaguer, T. Herranz, C. Weis, H. Bluhm, M. Salmeron, Langmuir 24 (2008) 9474–9478.
[35] M. Roiaz, E. Monachino, C. Dri, M. Greiner, A. Knop-Gericke, R. Schlogl, G. Comelli, E. Vesselli, J. Am. Chem. Soc. 138 (2016) 4146–4154.
[36] M.K. Gnanamani, G. Jacobs, R.A. Keogh, W.D. Shafer, D.E. Sparks, S.D. Hopps, G.A. Thomas, B.H. Davis, Appl. Catal. A Gen. 499 (2015) 39–46.
[37] Y. Dai, F. Yu, Z. Li, Y. An, T. Lin, Y. Yang, L. Zhong, H. Wang, Y. Sun, Chin. J. Chem. 35 (2017) 918–926.
[38] P. Zhai, C. Xu, R. Gao, X. Liu, M. Li, W. Li, X. Fu, C. Jia, J. Xie, M. Zhao, X. Wang, Y.W. Li, Q. Zhang, X.D. Wen, D. Ma, Angew. Chem. Int. Ed. 55 (2016) 9902–9907.
[39] I.C. Yates, C.N. Satterfield, Energy Fuels 5 (1991) 168–173.
[40] G.D. Weatherbee, C.H. Bartholomew, J. Catal. 77 (1982) 460–472.
[41] S. Neatu, J.A. Macia-Agullo, P. Concepcion, H. Garcia, J. Am. Chem. Soc. 136 (2014) 15969–15976.
[42] C.H. Wu, B. Eren, H. Bluhm, M.B. Salmeron, ACS Catal. 7 (2017) 1150–1157.
[43] T. Ishida, T. Yanagihara, X. Liu, H. Ohashi, A. Hamasaki, T. Honma, H. Oji, T. Yokoyama, M. Tokunaga, Appl. Catal. A Gen. 458 (2013) 145–154.
[44] M. Khobragade, S. Majhi, K.K. Pant, Appl. Energy 94 (2012) 385–394.
[45] M. Blanchard, H. Derule, P. Canesson, Catal. Lett. 2 (1989) 319–322.
[46] K.H. Cats, B.M. Weckhuysen, ChemCatChem 8 (2016) 1531–1542.
[47] A.C. Ferrari, J. Robertson, Phys. Rev. B 64 (2001) 075414.
[48] G. Prieto, A. Martínez, P. Concepción, R. Moreno-Tost, J. Catal. 266 (2009) 129–144.
[49] M. Sadeqzadeh, H. Karaca, O.V. Safonova, P. Fongarland, S. Chambrey, P. Roussel, A. Griboval-Constant, M. Lacroix, D. Curulla-Ferré, F. Luck, A.Y. Khodakov, Catal. Today 164 (2011) 62–67.
[50] J. Paterson, M. Peacock, E. Ferguson, R. Purves, M. Ojeda, ChemCatChem 9 (2017) 3463–3469.
[51] M.K. Gnanamani, G. Jacobs, W.D. Shafer, B.H. Davis, Catal. Today 215 (2013) 13–17.
[52] N.E. Tsakoumis, M. Rønning, Ø. Borg, E. Rytter, A. Holmen, Catal. Today 154 (2010) 162–182.
[53] A.M. Saib, D.J. Moodley, I.M. Ciobîcă, M.M. Hauman, B.H. Sigwebela, C.J. Weststrate, J.W. Niemantsverdriet, J. van de Loosdrecht, Catal. Today 154 (2010) 271–282.